

Three-dimensional Forming of Multi-layered Materials: Material Heat Response and Quality Aspects

Sami-Seppo Ovaska*

Lappeenranta University of Technology

Pavel Geydt

Lappeenranta University of Technology

Ville Leminen

Lappeenranta University of Technology

Johanna Lyytikäinen

Lappeenranta University of Technology

Sami Matthews

Lappeenranta University of Technology

Panu Tanninen

Lappeenranta University of Technology

Malte Wallmeier

Technical University of Dresden

Marek Hauptmann

Technical University of Dresden

Kaj Backfolk

Lappeenranta University of Technology

ABSTRACT

The micro- and macrostructural changes occurring in multi-layered substrates during three-dimensional forming were studied by atomic force microscopy (AFM), scanning electron microscopy (SEM) and optical analyses. Particular attention was paid to heat-induced deformations at the interface between of polymeric coating layer and the paperboard. With excessive heat transfer, occasional delamination of polyethylene terephthalate (PET) coating from the paperboard was observed. The mechanism behind delamination was studied in detail in-situ with an AFM at temperatures relevant to the converting process. Based on the analysis, the delamination could partially be linked to the widening of the initially-existing nano-scale cracks at the coating-paperboard interface due to the high temperature, rigid and less adhesive PET crystallites close to the paperboard layer, and the emergence of fissures and tensile stresses in the coating. SEM images also revealed severe macro-scale delamination in the paperboard matrix after forming. However, the results were somewhat conflicting, since optical and machine vision analyses showed indisputably that both the visual quality and the dimensional accuracy of formed trays were better at the higher forming temperature.

KEY WORDS

Atomic force microscopy, deep drawing, delamination, extrusion coating

***Sami-Seppo Ovaska**

Corresponding Author

sovaska@lut.fi

INTRODUCTION

Fiber-based products present a recyclable, printable and environment-friendly alternative to plastic packages in several product segments, including both food and non-food applications, but challenges in material forming are more apparent than with polymeric substrates. Several authors have studied three-dimensional forming and the behavior of paperboard during forming processes [1-8]. The extensibility of fiber-based substrates is much smaller than that of polymer materials [1, 2], suggesting that their forming into three-dimensional shapes is more difficult. Examples of such three-dimensional products are cups, plates and trays [1-3, 5]. Moreover, achieving a visually appealing appearance and a flat surface is much more challenging due to the wrinkling tendency of fiber-based materials, which is due to the material properties of paperboard [1, 2, 9]. In deep-drawing of paperboard materials, the wall of a three-dimensional object experiences a z-directional compression early after it has been drawn into the cavity (Fig. 1), which is a cylindrical bush with a clearance less than the material thickness to the punch.

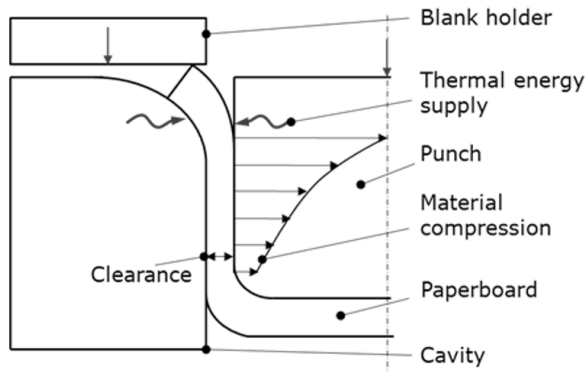


Fig. 1: Schematic illustration of the process conditions during deep drawing of paperboard [10].

Quality analysis of formed objects with regard to visual appearance and dimensional accuracy has been carried out by e.g. [9, 11]. Both these studies present investigations of formed products with optical image analysis systems, and visual comparisons have also been made [5]. Formability results have also been compared with finite element analysis (FEA) [12, 13]. In addition, the surface smoothness of formed objects can be determined with a 3D-profilometer [14]. Previous results show that a large number of wrinkles and a small distance between them is favorable for achieving visually appealing, evenly formed trays with the deep-drawing method [1, 9].

Recent advances in the deep-drawing of paperboard materials include the utilization of a flexible servo-hydraulic press [15, 16], which makes it possible to control the forces in the blank holder. The blank holder force has been found to be a focal process parameter that also affects the quality of deep-drawn paperboard shapes [1] and it can be increased without harming the material if the coefficient of friction between the forming cavity and the substrate is lower than that between the punch and the substrate [17]. The improvement is evident as a reduced wrinkle distance and increased uniformity of the wrinkles. A more uniform and fine distribution of wrinkles also eliminates discoloration in the wrinkles and is therefore an established quality criterion for the visual quality of three-dimensional shapes. These shapes also provide the basic capability for the products to achieve a gas-tight seal [18], as in the case of press-formed shapes [19]. However, the geometry and the height of the shapes that can give a gas-tight seal is strongly dependent on the formability of the paperboard.

The significance of heat on the formability of paperboard in a three-dimensional converting process is known well [20, 21] and better formability can be expected with a higher tool temperature, but heat exposure may also lead to quality problems. The combined effect of temperature and moisture on the elongation of fiber-based materials has been discussed by Kunnari et al. [22], who found that varying the moisture and/or temperature can increase the elongation by 2–2.5 percentage points. Heat has a major influence on the dimensions and rigidity of press-formed paperboard trays, and it is generally beneficial to pursue a high heat input in the forming process [11]. Heating has also been reported to be the most important parameter influencing the shape accuracy of deep-drawn paperboard objects [23]. Shape accuracy and the outer dimensions of formed products are critical factors, because too large a deviation in the dimensions can cause significant problems e.g. when the packages are heat-sealed [11]. Vishtal et al. [20] stated that the optimal temperature in deep drawing of paperboard would be 140–180 °C for the cavity and 60–100 °C for the die. However, optimal temperatures depend not only on the fiber material but also on the coating, which often sets limits to the temperature of the forming molds. Heat softens the plastic coating, which seals the creases in the corners of the tray [5, 24], and this affects the final rigidity of the tray and the flatness of the sealing surface [19]. Previous work, does not, however, do not describe the actual heat-related phenomena in the board material or its coating, although it is known that the thermo-mechanical history of polyethylene terephthalate (PET) affects its barrier properties [25]. Thermal exposure may also increase the crystallinity of polymeric materials, resulting in improved barrier properties [26].

The objective of the present work was to gain a deeper understanding of the effect of heat on the material performance in a three-dimensional forming process. The formability and dimensional stability of the cylindrical trays were evaluated by optical measurement techniques. The heat response of the substrates was characterized by e.g. surface free energy determinations at temperatures relevant to the converting processes and atomic force microscopy (AFM) that made it possible to observe changes caused by the temperature shift. The different delamination mechanisms of polymeric coatings and bulk matrix (paperboard) occurring during forming are discussed. This work is a continuation of our earlier paper [10], in which we discussed the relationship between mould clearance and the distribution of wrinkles using partly the same paperboards as in this study.

MATERIALS AND METHODS

Substrates and deep-drawing experiments

Seven conditioned (23 °C, RH 50%) commercial paperboards from different manufacturers were converted into cylindrical trays using a pilot-scale deep drawing machine. The structure of the machine has been described in earlier publications [1, 27]. The converting was carried out at two forming temperatures (100 °C and 180 °C) with a constant drawing velocity (25 mm/s) and a constant blank holding force (1500 N). The blank holding force was selected based on the durability of the weakest material (2 – pigmented), but e.g. material 1 - PE withstood a blank holding force of 10 000 N without any defect, which indicates a significant difference between the materials. The physical properties of substrates are given in Table 1. Bulk was determined in accordance with ISO 534:2011. Tensile index (TI) and strain-at-break (SAB) values were measured in accordance with ISO 1924-3:2005.

Table 1: Description of the commercial paperboard samples.

Sample	Coating ¹	Grammage, [g/m ²]	Bulk, [cm ³ /g]	TI (MD/CD), [Nm/g]	SAB (MD/CD), [%]
1 – PE	PE 60 + Internal PE layer 5	365	0.89	71.9/37.5	14.5/9.7
1 – uncoated	-	200	1.35	77.6/41.9	13.2/8.2
2 – pigmented	Pigment coating	250	1.41	51.0/30.4	1.6/3.7
3 – PET	PET 40	330	1.07	69.5/36.4	1.7/4.5
3 – uncoated	-	290	1.08	78.4/37.0	1.8/4.9
4 – PET	PET 40	390	1.06	76.0/35.0	2.2/4.4
4 – uncoated	-	350	1.09	75.2/38.4	2.0/4.5

¹Number after coating type denotes coat weight [g/m²].

Heat-induced changes in paperboards

Surface energies of the samples were determined with an optical tensiometer (Attension Theta, Biolin Scientific AB), equipped with an electrically heated measurement chamber. The probe liquids were deionized water, ethylene glycol (VWR S.A.S. International, France) and 99% diiodomethane (Alfa-Aesar GmbH & Co KG, Germany). All the paperboard samples were conditioned at 23 °C and 50% relative humidity before measurement.

The contact angles were determined at 25, 50, 75, and 100 °C. The measurement chamber was heated to the required temperature and the temperature of the sample was allowed to stabilize for five minutes. A drop of test liquid (3 µl of deionised water, 3 µl of ethylene glycol or 1 µl of diiodomethane) was placed on the surface of the sample using an automatic dispenser. Contact angles were reported as average values of five independent measurements. From each measurement, the contact angle value was taken from the point where contact angle had decreased by 5–10% from the initial contact angle. Surface energies were calculated using the Lewis acid-base approach.

Analysis of interaction of PET and paperboard on nanoscale at the cross-cut

Atomic force microscopy (AFM) investigations were carried out with a Multimode 8 (Bruker, USA) device on material 4 – PET. Additional data were acquired with a Nikon OMV-UNIV optical microscope with video camera assembled into the AFM system, which allowed an optical magnification of 200x. A thermal application controller TAC with heater/cooler module CLS200 (Watlow, USA) and digital readout was applied to heat the sample with a precision of 0.1 °C. All AFM investigations were done with appropriate sample/probe holders, mechanical/thermal noise damping and specified AFM probes.

Five types of probes were utilized in this work: (1) Scanasyst-Air with a spring constant (k) of 0.4 N/m, tip radius (r) approx. 5 nm, resonant frequency (f) of approx. 70 kHz for studies of topography and roughness; (2) PFTuna with k = 0.6 N/m, r ≈ 30 nm, f ≈ 70 kHz for measurements of surface electric potential; (3) NCHV with k approx. 40 N/m, r ≈ 15 nm, f ≈ 320 kHz for thermal studies, and two types of probe were calibrated by the necessary protocol to make possible the measurement of Young's modulus: (4) TAP525a with f = 447 kHz, deflection sensitivity 33 nm/V, quality factor Q 600, k = 133 N/m, r

= 20 nm (for quantitative elastic studies for materials with a modulus of up to approx. 20 GPa) and (5) NCHV-A with $f \approx 370$ kHz, $k = 74$ N/m and $r \approx 15$ nm (for studies up to approx. 4 GPa). A Quantitative NanoMechanics (QNM) mode of AFM investigation was utilized to evaluate the elastic parameters of the sample. Probes were calibrated in Nanoscope 1.50 software firstly by an Absolute method requiring estimation of the spring constant for probes with cantilevers stiffer than 1 N/m by the Sader method [28], and secondly by a relative method where standard calibrating test material, i.e. a flat polystyrene film, was measured and the calibration verified by the established tunings of elasticity.

AFM imaging was done in the PeakForce Tapping regime with a scan rate of 0.1 Hz and a resolution of 512x192 pixels. Measurement settings used for the modes were: (1) PeakForce setpoint force PF 1 nN, image size S 2x2 μm , amplitude PF_a 100 nm and frequency of oscillation PF_f 2 kHz for topography and roughness; (2) PF 1 nN, S 10x10 μm , PF_a 150 nm, PF_f 1 kHz and Lift height of the second pass above the surface 60 nm for surface potential; (3) PF 10 nN, S 20x20 μm for matching zones found in surface morphology after heat exposure, PF_a 150 nm, PF_f 2 kHz for the thermal experiment; (4) PF 60 nN, S 5x5 μm , PF_a 80 nm, PF_f 2 kHz for elastic measurements in QNM mode. A significant force of 60 nN was necessary to establish the appropriate local pressure and depress the surface by 1 nm as prescribed for the QNM mode.

A cross-sectional cut of the sample 4 – PET was achieved with a broad-ion-beam (BIB) cutting machine to reveal the PET-paperboard interface. A special cross-sectional AFM sample holder SD-103 (Veeco, USA) was utilized to fix the sample normal to the AFM cantilever, while paperboard was on the side of a plastic screw. The rate of temperature change in thermal experiments was 1°C/min for heating and either 3 °C/min or 1 °C/min for fast and slow cooling, respectively. Raw AFM data were processed

in Nanoscope 1.50 software. Topography undergone corrections by 0th order profile flattening and by 1st order plane were fitted only where necessary and so as not to mislead the topography and its roughness. Results for elastic measurements, including a histogram of Young's modulus, were obtained after the profile flattening of the 0th order to collect significant statistical information from the larger studied area and for illustrative purposes. The differences between the peak positions for the separate phases remained unchanged after such processing. The position of the highest peak has been later aligned to the average value observed from the unprocessed data from the corresponding regions of the sample's ambient PET matrix material. Equivalent values were observed on corresponding locations assumed to be PET inclusions by two different types of probe (TAP525a and NCHV-A) and across these inclusions, so that values were later found to be repeatable.

In addition to the AFM imaging, micrographs were taken from selected materials with a scanning electron microscope (SEM) in order to examine macro-scale delamination.

Quality analysis of deep-drawn trays

The precise measurement of the location of wrinkles on the flange is necessary for an objective evaluation of the optical quality of a deep-drawn tray. A Toolscan® R360 (Laboratory Imaging s.r.o.) was utilized for image acquisition of the wrinkled area of the tray flange. The device was equipped with an Imaging Source DMK 51AU02 industrial camera and an IB/E TZ 16-0.5-100 telecentric lens. The system took high-resolution images of small parts of the flange and rotated the sample to cover the whole surface of the scanned object. Afterwards, the software stitched the images together, similar to a panorama image, to produce a continuous picture of the whole flange of the sample. A small region of an image of the flange is shown in Fig. 2.

The wrinkles cannot be directly detected in the raw image in Fig. 2a. Different steps of image processing are necessary to emphasize the wrinkles. In the first step, random dark spots, due to the uneven surface of the paperboard and noise in the image are reduced using a median filter. The median filter calculates a mean value of a defined region around each pixel and replaces the value of the center pixel with the mean value of the neighborhood. A Sobel edge detection filter is then used to produce images where the black-white transition in a wrinkle is enhanced. The resulting image can then be binarized to produce a monochrome image based on a threshold value. Afterwards, the morphological image processing operations of opening, closing and dilation are applied to enlarge the white regions of the detected wrinkles. The result is shown in Fig. 2b, and it makes possible to detect the white areas in Fig. 2b automatically. To achieve this, the picture is scanned vertically in several lines, the white regions are detected and each point of detection is automatically marked with a dot (Fig. 2c).

Shape determination with a machine-vision-based system

The manufactured trays were analyzed with a machine-vision-based quality monitoring system. Each tray was photographed with a Cognex IS5605-11 camera. Background light was used to enable

accurate measurement of the dimensions. Images were taken 650 mm above the tray bottom to prevent image distortion. The camera takes black and white images with a resolution of 2456 x 2048. A single pixel is equivalent to an area of 0.017 mm x 0.017 mm on the monitored surface.

The vision software recognizes patterns and automatically calculates the dimensions of the measured object. The precision of the monitoring method was tested by measuring the same sample ten times using slightly different orientations. The standard deviation of the measurements was approx. 0.05 mm. The outer and inner dimensions of the deep-drawn objects were measured, and the difference between the diameters was calculated to evaluate shape distortion. A more detailed description of the machine vision system has been presented by Tanninen et al. [11].

RESULTS AND DISCUSSION

Effect of ambient temperature on the surface free energy

The surface energies of uncoated, pigment-coated, PET-coated and polyethylene (PE)-coated paperboards were determined on a temperature scale relevant to deep-drawing of fiber-based substrates [20] to evaluate the effect of temperature on

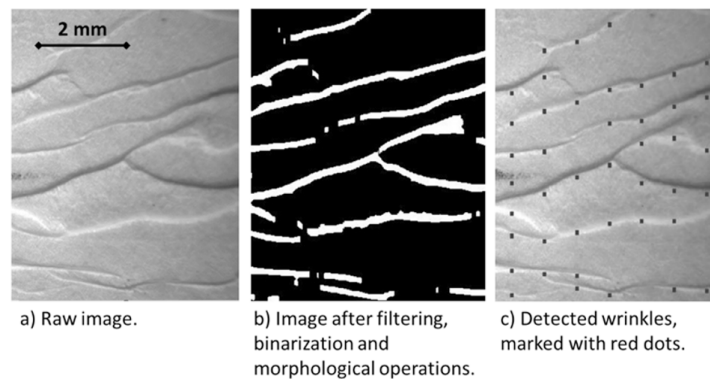


Fig. 2: Digital image editing and detection of wrinkles [9].

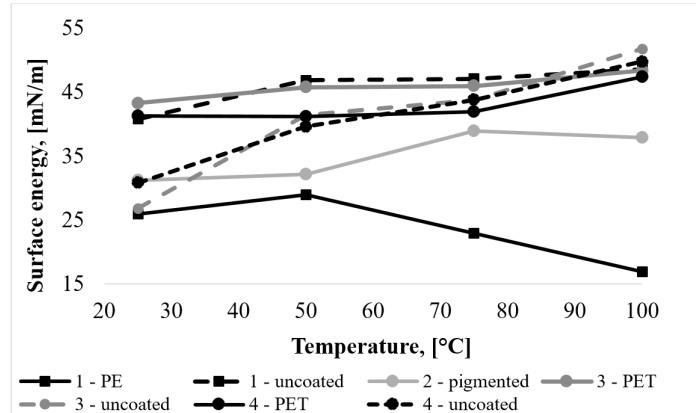


Fig. 3: Surface energies of paperboard and coatings at different temperatures.

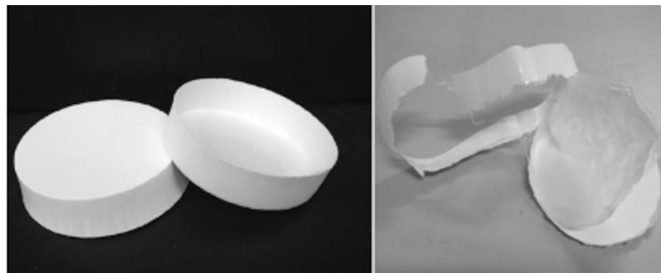


Fig. 4: Examples of faultless cylindrical trays (left) and a broken tray with delaminated plastic coating.

the surface energy. With increasing temperature of the substrate, the surface energy of sample 1 - PE decreased while the surface energy of PET-coated paperboards increased. An increase in surface energy were also recorded with uncoated boards and the pigment-coated sample. The pigment-coated sample responded to increased temperature more slowly than the other samples, the increase occurring at 75°C. The results are shown in Fig. 3.

PET and PE are semi-crystalline polymers. The degree of crystallinity of PET has been reported to be 30–35% depending on molecular weight and of PE 45–60% [29, 30]. The glass transition temperature (T_g) of PET has been reported to range from 67 to 140°C depending on e.g. the degree of crystallinity [31]. A PET coating is also hydrophilic, and evaporation of free water from the coating layer due to heat might partially explain the observed increase in surface energy. Other possible explanations may

include e.g. molecular reorientation due to e.g. thermal shrinkage and changes in crystallinity occurring in a heated environment [26]. The hydrophobic nature of the PE coating resulted in a lower surface energy than that of the PET coating. The lower surface energy of the PE-coated sample when the temperature was increased may be due to e.g. a change in the degree of crystallinity. The surface energy of the pigment-coated board was lower than that of the PET-coated samples. This was also seen at higher temperatures, and it was ascribed to a movement of synthetic latex binder due to heat [32].

Nano-scale delamination of the coating layer

A rare defect during the forming trials was the delamination of the extrusion-coated PET-layer from the paperboard (Fig. 4). This took place when the heat exposure was long (drawing velocity 2 mm/s) and the tool temperature was 180°C, which

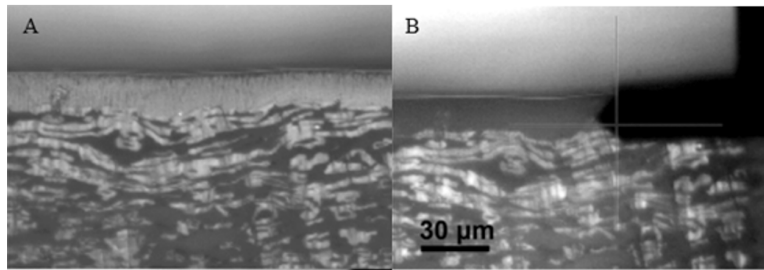


Fig. 5: Optical microscope images of PET-paperboard interface at 25°C. PET is seen as white (A) before thermal treatment, but as dark (B) after two cycles of heating/cooling.

emphasizes the significance of optimizing the heat transfer to the material in the converting stage. It has been suggested that heating the paperboard substrate before coating, e.g. by using flame corona, may promote the adhesion between the PET and the paperboard [33]. Other possibilities for obtaining better adhesion between the extrusion coating and the paperboard include surface treatment with electric corona or plasma and the introduction of a copolymer that increases the adhesion strength [33]. The exact mechanism behind delamination of the coating layer in a forming process is not, however, completely understood, but it can be related to blistering due to the rapid evaporation of water.

To gather more information about the mechanisms behind delamination, broad-ion-beam-cut cross-sections of PET-coated paperboard were imaged with an AFM at temperatures relevant to the converting process. The border between the polymer coating and the paperboard was visible on a cross-sectional cut with an optical microscope (Fig. 5). The thickness of the PET layer was approx. 20 µm. At the same time, the thickness of the borderline between the PET and paperboard was approx. 10 nm, as it was later registered by AFM.

Such an abrupt transition from paperboard to polymeric coating appears to be one of the factors affecting the adhesion between PET and paperboard. Comparison of the contact area before and after heating (Fig. 6) revealed a significantly more pronounced border between PET coating and a paperboard after heating. In addition, the angle between the materials increased approx. seven

degrees and wavy lines became noticeable in the topography of PET coating upon heating from 25°C to 95°C. These changes persisted when the sample was cooled back to 25°C. Wavy hills with a height of approximately 30 ± 10 nm resulted in a drastic increase in the local root-mean-square (RMS) roughness from 11 nm to 53 nm (for 8×8 µm area, with a pixel size of 40×100 nm) after the first heating cycle followed by fast cooling. The arrays of extended nanohills were oriented imperfectly perpendicular to the border between the two materials, indicating a significant difference in thermal expansion. In addition, a RMS-specific change in brightness was observed in the PET layer with an optical microscope during the thermal treatment, due to a reduction in reflectance of the PET surface as it became rougher. Such a change in brightness was partly recoverable, and was affected by the cooling rate.

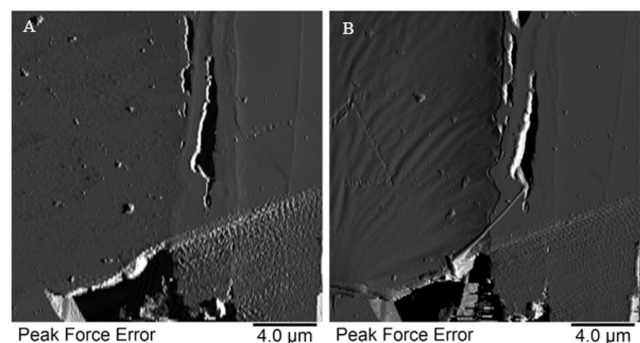


Fig. 6: AFM images of the PET-paperboard interface at 25°C. The PET surface (locating left side of the images) was flat before thermal treatment (A) but the surface became covered with nanohills after first heating to 95°C (B).

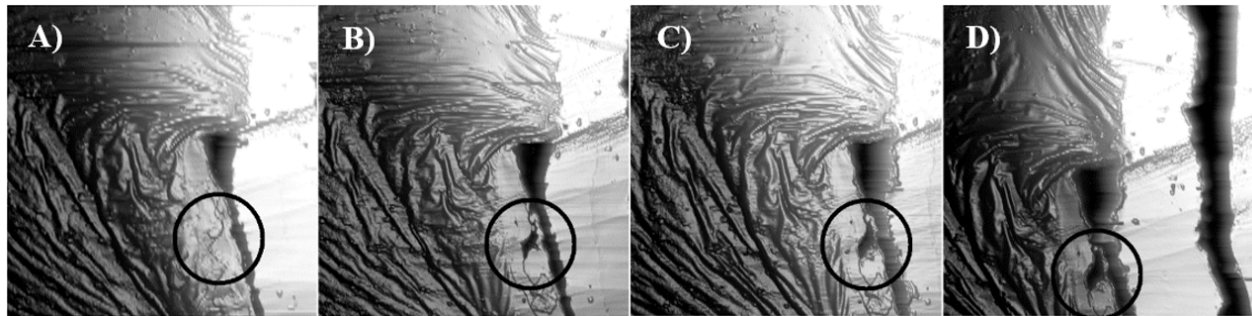


Fig. 7: Top view 3D-AFM topography images of 20x20 μm area of PET-paperboard interface at different temperatures in the second heating/cooling cycle: (a) 25°C; (b) 70°C; (c) 95°C and (d) 30°C. The circle shows the location at which a single fracture emerged.

From a converting technology perspective, it is important to determine the temperature at which the nanocracking begins. AFM analysis revealed that existing fissures at the surface became wider already at 70°C. The width of the nanocrack on Fig. 6 increased from 2.4 μm to 2.6 μm upon first heating to 95°C. This change was irreversible, i.e. the width of the fracture retained the same after the sample was cooled back to 25°C. Additional fractures emerged in the coating layer close to the interface and remained in the PET after cooling. The growth and fixing of the fracture is visible in Fig. 7, where the same location was examined at 25°C, 70°C, 95°C and 25°C during the second heating series followed by slow cooling, i.e. a cooling rate of 1°C/min. These factors caused a disturbance of the initially flat surface of the PET on the examined cross-sectional cut. It seems remarkable that the roughness evaluated for the paperboard (6x6 μm area, with pixel size 40x100 nm) increased from 10 nm to only 17 nm.

Considering such irreversible changes in the morphology of the sample, it can be suggested that heat exposure leads to the release of tensile stresses in the coating layer. Tensile stresses in close proximity to the PET-paperboard interface were ascribed to uneven thermal expansion, i.e. to an order of difference in the coefficients of

thermal expansion for PET and paperboard [34, 35]. Further insight into the changes in morphology observed at the interface between PET and paperboard can be achieved by considering the difference in moisture content of the two materials. PET is a hygroscopic material, but paperboard had an even higher moisture content in the room environment. When the sample was heated the water extensively evaporated through the surface and led to uneven changes in the volume of the two materials. PET is a semi-crystalline polymer, and crystallites can be seen with a microscope (Fig. 8). The coefficient of thermal expansion of the PET crystallites is not known, but the density of the crystalline phase is about 11% higher than that of the amorphous phase. The phase transition of the amorphous material occurs above 67°C, so the ratio of crystallite to amorphous phase can change substantially. Thus, all the mentioned factors extensively affected the tensile force inside the materials and at their interface, and such changes in morphology can be partly reversible.

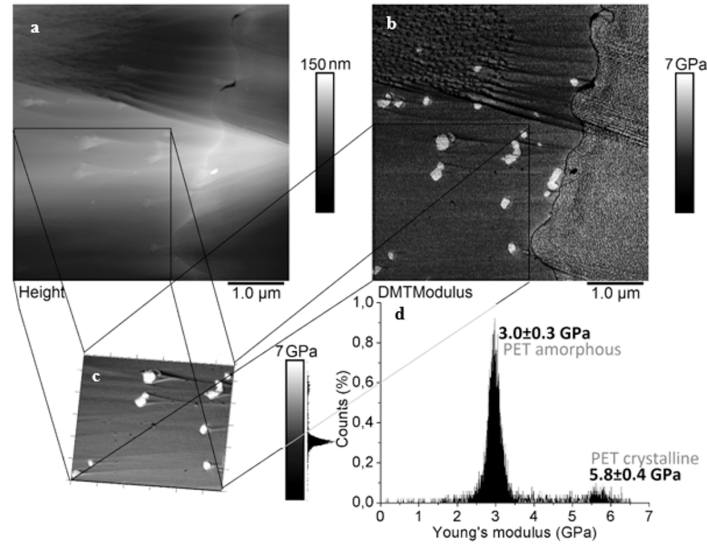


Fig. 8: Illustration of mapping of elasticity for calibrated QNM mode measurement. (a) AFM topography of the PET-paperboard interface with droplet-shaped inclusion. (b) DMT channel of modulus calculated by the Derjaguin-Muller-Toporov (DMT) model of elastic contact. Inclusions have rigid round cores seen as bright spots on the left part of the image. The right part shows the paperboard. (c) Dimensional inset of 3D topography in real axis scales overlaid by a color scheme from the elastic channel to highlight the rigid crystallites. The color bar shows the distribution of values on the elastic map. (d) Histogram of elasticity on a selected area of (c) showing the counts of exact values. The first peak is associated with amorphous PET, and the second peak is associated with PET crystallites

In order to prove the existence of PET crystallites near the border between PET and paperboard, a quantitative investigation in the QNM mode was carried out. An AFM probe calibrated with an extraordinary spring constant of the cantilever was used to deform the surface of the cross-sectional cut near the interface. It was previously evident in the topography that the PET area continues the inclusions (Fig. 6). They had a droplet-shape and were protruding approx. 6 nm above the flat surface of the BIB cut. It was also evident upon application of the stiff NCHV-A probes that only the cores of these droplet-shaped inclusions were rigid. The composition of the PET, the amount of inclusions and their higher rigidity suggests that these were PET crystallites (Fig. 8). The diameter of these crystallites was 100–200 nm. They were less adhesive than

the amorphous PET phase; the difference in local adhesion between the amorphous PET and the crystallites was measured by the AFM probe to be 0.8 nN. Young's modulus of the PET crystallites was found to be 5.8 ± 0.4 GPa. This value has not previously been reported and was acquired simultaneously with the elastic modulus of 3.0 ± 0.3 GPa of PET and 4.7 ± 0.7 GPa for paperboard.

Determination of the surface electric potential in two-pass Kelvin force microscopy led to the observation of a slightly positive electric potential on most of the PET crystallites; the excess was approximately 0.2 V (not shown here). Such an effect can be explained by space charges. Since the impact of the PET crystallites on stresses in the PET-paperboard interface has not been fully established, a detailed further examination is required.

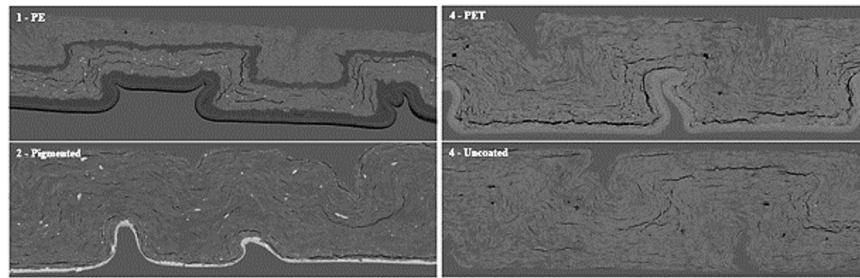


Fig. 9: Cross-sectional SEM-images of selected paperboards.

Although, the decline in chemical attachment and mechanical stability of the PET-paperboard interface when heated has now been observed on a nanoscale by QNM mode. The emergence and enlargement of the fractures near the interface, which is caused mainly by uneven expansion, may result in a partial detachment of the polymer material from the fibers and led to the observed abrupt edges of the fractures. All this leads to the suggestion that extensive heat transfer should be avoided in converting processes in order to minimize the risk of coating layer delamination.

Internal macro-scale delamination tendency

Cross-sectional scanning electron micrographs of tray walls revealed substantial differences in internal macro-scale delamination between the studied materials (Fig. 9). Delamination occurred between the two PE layers in material 1, but the outer paperboard layer remained almost unchanged. The adhesion between PE and paperboard was not affected by deep-drawing as in the case of material 4 – PET, in which severe delamination took place beneath the coating layer and also in the bulk matrix. The PET coating did not, however, affect the degree of delamination in the bulk region, since the changes there were similar to those in the corresponding uncoated material. The pigment-coated board showed only minor delamination in the internal region, which was ascribed to its lowest density (see Table 1 for details), but more intense delamination took place close to the coating layer. Material performance in deep-drawing seems

thus to be affected by its specific volume, i.e. bulk; high bulk promotes good quality due to the small distance between the wrinkles (see Fig. 10) and it also reduces material delamination in the bulk region. The specific volume on the other hand does not necessarily affect the delamination tendency of the coating layer nor the depth or width of the wrinkles (cf. materials 2 and 4 – PET), both of which are affected by the thickness of the coating layer (cf. materials 1 – PE and 4 – PET).

Visual appearance of deep-drawn trays based on wrinkle analysis

The wrinkles extended lower in the flange area with plastic-coated materials with a forming temperature of 100°C (Fig. 10). The distance between the wrinkles was between 0–20 mm in materials 1 – uncoated, 1 – PE and 2 – pigmented, indicating a better visual quality, but the performance of materials 3 and 4 was poorer regardless of whether or not there was a PET coating. The results thus suggest that PET-coated materials require more intense heating, probably due to differences in material stiffness and thickness, and selecting a higher forming temperature is advisable. With a forming temperature of 180°C (Fig. 11), the wrinkles extended to almost the whole flange area, the distances between the wrinkles were overall smaller than at 100°C forming temperature, and clear peaks were noticed only in trays made from materials 1 – PE and 4 – PET. The better formability of uncoated materials was expected, since the lack of a plastic layer increases the ability of internal AKD sizing to improve the material formability [36].

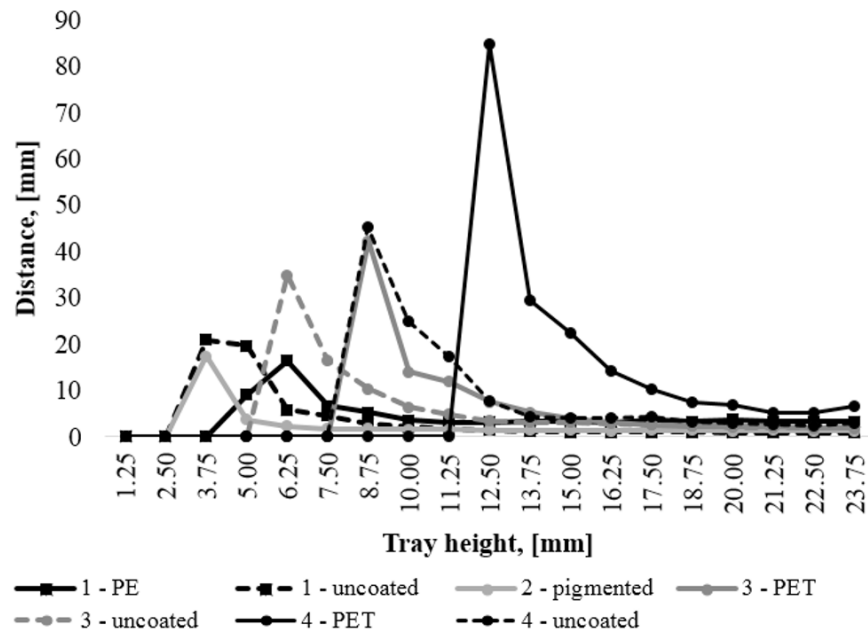


Fig. 10: The distance between the wrinkles as a function of tray height. The forming temperature was 100°C and the drawing velocity was 25 mm/s.

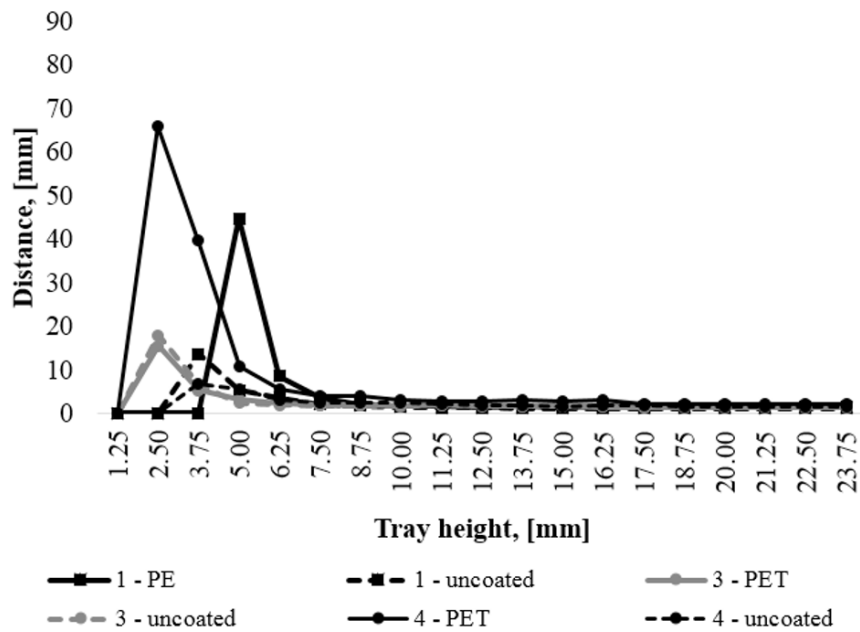


Fig. 11: The distance between the wrinkles as a function of tray height. The forming temperature was 180°C and the drawing velocity was 25 mm/s.

The distance between the wrinkles in trays made from material 2 – pigmented was short in all parts of the tray wall with a forming temperature of 100°C. This was ascribed to a lower tensile strength and bending stiffness, both of which are indicators of better formability [36]. This material also had the highest specific volume, which is an indicator of a less compact structure that has been reported to result in considerably long wrinkles in deep-drawing [36]. However, increased stickiness onto tools impaired the processability of material 2, which was ascribed to melting of the latex binder, and it was found to be extremely difficult to make parallel trays. This made it impossible to analyze material performance in a reliable manner and the distance between the wrinkles is not reported here.

The diagrams clearly show that the coating layer clearly influenced the wrinkling behavior and it can be interpreted that an extruded polymer coating contributes in two ways to the reduction of wrinkle distances. The bending stiffness increases to some extent so that the compensation for excess material shifts to a deformation between already initiated wrinkles rather than to the initiation of a new wrinkle. The material displacement under the blank holder orthogonal to the wrinkles is also affected by the friction of the coating layer against the blank holder. Since pigment-coated material showed the shortest distance between the wrinkles at a forming temperature of 100°C, it can be assumed that the friction differed from the other substrates or that the coating became softer at a lower temperature than the other polymer coatings.

It should also be noted that the blank holding force used (1500 N) was relatively low, which may explain the poor performance of materials 3 and 4 at 100°C [1] that withstood much greater blank holding forces (6500–9500 N). Although a higher forming temperature indisputably improved the shape accuracy of deep-drawn objects [9] and it was found that the deep-drawing process

generally suits the studied substrates well, the results suggest that optimization of the parameters is required particularly with plastic-coated materials and it is obviously advisable to use a low forming temperature for pigment-coated boards.

Dimensions of deep-drawn trays

The difference between upper and lower diameters (Δd) of the flange was greatly affected by the forming temperature (Table 2). Higher forming temperature decreased the Δd value of trays made from PE-coated paperboard by 9.1 mm, which can be considered to be a remarkable improvement in dimensional quality, and was ascribed to greater rigidity [11]. In addition, trays made from PET-coated paperboards, material 3 – uncoated, and material 2 – pigmented showed smaller Δd values at a tool temperature of 180°C. The dimensions of trays made from material 4 – uncoated suffered from higher forming temperature, but the validity of this observation was questionable when the standard deviations were taken into consideration. The high distortion of the flange and the undesired oval shape of trays made from material 1 – uncoated made it impossible to determine the Δd values with this machine-vision-based technique, suggesting that the coating layer contributes to shape accuracy and dimensional stability. However, a further study is needed to clarify the role of material moisture content on material performance and tray dimensions, since the mechanical properties of paperboard are strongly affected by the moisture content [37] and the initial moisture content affects the stiffness of paperboard trays [38].

Table 2: Δd values and their standard deviation and difference for cylindrical trays. The Δd_1 value is the difference between the upper and lower diameters of trays formed at a tool temperature of 100°C, and Δd_2 with a tool temperature of 180°C.

Material	Δd_1 (100°C), [mm]	σ (100°C)	Δd_2 (180°C), [mm]	σ (180°C)	$\Delta d_1 - \Delta d_2$, [mm]
1 - PE	16.2	2.0	7.1	2.1	9.1
2 - pigmented	18.0	1.0	17.5	0.6	0.5
3 - PET	17.2	0.6	15.1	0.0	2.1
3 - uncoated	23.0	3.3	16.5	4.5	6.5
4 - PET	12.8	1.4	6.0	3.2	6.8
4 - uncoated	11.7	2.2	12.1	3.6	-0.4

CONCLUSIONS

This study was focused on heat-related phenomena that occur when paperboard is formed into 3D shapes that can be used as e.g. food packages. The effects of forming temperature on material processability and tray quality were twofold. The heat sensitivity of PE and pigment coatings made the materials stickier, which not only increased the prevalence of defects in the trays, but also increased the need to clean the forming tools. Moreover, the AFM analysis of cross-sections of PET-coated material revealed the formation of fissures at the PET-paperboard interface and the nano-scale delamination of the coating layer from the paperboard. These phenomena occurred at relatively low temperatures and led to an observable deterioration in the attachment of the two materials. However, the defects occurred over a limited area and their influence on the overall performance of the coating was negligible, although the imaging provided plenty of novel scientific information on interfacial phenomena at high temperatures. A more severe delamination occurred in the bulk matrix, probably due to mechanical forming forces.

Wrinkle analysis clearly showed a better formability and more accurate tray dimensions at the higher forming tool temperature. A higher forming temperature seems particularly advisable for plastic-coated substrates. The wrinkles were much shorter with PET-coated paperboards than for the same materials without a coating at a tool temperature of 100°C. Increasing the forming temperature to 180°C eliminated the difference between uncoated and plastic-coated samples, but this is definitely not suitable for pigment-coated substrates, which showed good visual quality after forming at the lower temperature. In addition, multilayer structures can be problematic, since the trays can be distorted. This suggests that the layer structure should be as simple as possible.

The heat responses of the different types of paperboard materials described in this study can provide answers to questions of material selection and process optimization, particularly if the results are combined with mechanical analyses such as friction measurements at temperatures relevant to the converting process. All of the aforementioned are interesting topics for further research. The results also emphasize the importance of having sufficient adhesion between the different layers of multi-layered composite materials in order to avoid delamination problems.

REFERENCES

- [1] M. Hauptmann and J. Majschak, "New quality level of packaging components from paperboard through technology improvement in 3D forming," *Packag. Technol. Sci.*, vol. 24, (7), pp. 419–432, 2011.
- [2] A. Vishtal and E. Retulainen, "Deep-drawing of paper and paperboard: the role of material properties," *Bioresources*, vol. 7, (3), pp. 4424–4450, 2012.
- [3] P. Tanninen, H. Lindell, E. Saukkonen and K. Backfolk, "Thermal and mechanical durability of starch-based dual polymer coatings in the press forming of paperboard," *Packag. Technol. Sci.*, vol. 27, (5), pp. 353–363, 2014.
- [4] M. Hauptmann, S. Ehlert and J. Majschak, "The effect of concave base shape elements on the three dimensional forming process of advanced paperboard structures," *Packag. Technol. Sci.*, vol. 27, (12), pp. 975–986, 2014.
- [5] V. Leminen, P. Tanninen, P. Mäkelä and J. Varis, "Combined effect of paperboard thickness and mould clearance in the press forming process," *Bioresources*, vol. 8, (4), pp. 5701–5714, 2013.
- [6] X. Zeng, A. Vishtal, E. Retulainen, E. Sivonen and S. Fu, "The elongation potential of paper - How should fibres be deformed to make paper extensible?," *Bioresources*, vol. 8, (1), pp. 472–486, 2013.
- [7] V. Leminen, P. Tanninen, H. Lindell and J. Varis, "Effect of blank holding force on the gas tightness of paperboard trays manufactured by the press forming process," *Bioresources*, vol. 10, (2), pp. 2235–2243, 2015.
- [8] K. Scherer, "Untersuchungen über Ziehfähigkeit und den Ziehvorgang von Pappe," Ph.D. Dissertation, Technische Hochschule Dresden, Dresden, Germany, 1932.
- [9] M. Wallmeier, M. Hauptmann and J. Majschak, "New methods for quality analysis of deep-drawn packaging components from paperboard," *Packag. Technol. Sci.*, vol. 28, (2), pp. 91–100, 2015.
- [10] V. Leminen, S.-S. Ovaska, M. Wallmeier, M. Hauptmann, K. Backfolk and J. Varis, "Effect of material properties and drawing parameters on the quality of deep-drawn paperboard products," *Proceedings of the FAIM 2016 Conference*, Soul, South Korea, 8 p., 2016.
- [11] P. Tanninen, V. Leminen, M. Kainusalmi and J. Varis, "Effect of process parameter variation on the dimensions of press-formed paperboard trays," *Bioresources*, vol. 11, (1), pp. 140–158, 2016.
- [12] P. Groche, D. Huttel, P-P. Post, S. Schabel, "Experimental and numerical investigation of the hydroforming behavior of paperboard," *Prod. Eng. Res. Devel.*, Vol. 6 (3), pp. 229–236, 2012.
- [13] M. Wallmeier, E. Linvill, M. Hauptmann, J-P. Majschak, S. Östlund, "Explicit FEM analysis of the deep drawing of paperboard," *Mechanics of materials*, Vol 89, pp. 202–215, 2015.

- [14] V. Leminen, P. Mäkelä, P. Tanninen and J. Varis, "The use of chromatic white light 3D-profilometry in the surface quality analysis of press-formed paperboard trays," Proceedings of the 25th International Conference on Flexible Automation and Intelligent Manufacturing, 2015, Vol. II, pp.74-81.
- [15] M. Hauptmann, H. Lohse, J.-P. Majschak and S. Helduser, "Flexible Verpackungskomponenten durch mehrdimensionale Umformung von Papier und Karton," VV Tagung Verarbeitungsmaschinen und Verpackungstechnik, Technische Universität Dresden, Dresden, Germany, 2009.
- [16] H. Lohse, "Ziehen von Papier und Karton, Elektrohydraulisches Antriebssystem ermöglicht flexible Prozessgestaltung," O+P, Ölhydraulik und Pneumatik, Teil 1: (04), pp. 118-123, 2010; Teil 2: (05), pp. 192-196, 2010.
- [17] M. Hauptmann, J. Weyhe and J.-P. Majschak, "Optimisation of deep drawn paperboard structures by adaptation of the blank holder force trajectory," J. Mater. Process. Technol., vol. 232, pp. 142-152, 2016.
- [18] M. Hauptmann, "Gastight paperboard package - a new step in food packaging," Professional papermaking, (1), pp. 48-51, 2013.
- [19] V. Leminen, P. Mäkelä, P. Tanninen and J. Varis, "Leakproof heat sealing of paperboard trays - Effect of sealing pressure and crease geometry," Bioresources, vol. 10, (4), pp. 6906-6916, 2015.
- [20] A. Vishtal, M. Hauptmann, R. Zelm, J.-P. Majschak and E. Retulainen, "3D forming of paperboard: The influence of paperboard properties on formability," Packag. Technol. Sci., vol. 27, (9), pp. 677-691, 2014.
- [21] E. Linvill, S. Östlund, "The Combined Effects of Moisture and Temperature on the Mechanical Response of Paper," Experimental Mechanics, Vol. 54 (8), pp. 1329-1341, 2014.
- [22] V. Kunnari, P. Jetsu and E. Retulainen, "Formable paper for new packaging applications," 23rd Symp. International Association of Packaging Research Institutes (IAPRI), 2007.
- [23] M. Wallmeier, K. Noack, M. Hauptmann and J.-P. Majschak, "Shape accuracy analysis of deep drawn packaging components made of paperboard," Nord. Pulp Paper Res. J., vol. 31, (2), pp. 323-332, 2016.
- [24] V. Leminen, P. Mäkelä, P. Tanninen and J. Varis, "Methods for analyzing the structure of creases in heat sealed paperboard packages," J. Appl. Packag. Res., vol. 7, (1), pp. 49-60, 2015.
- [25] I. Özen, G. Bozoklu, C. Dalgıçdir, O. Yücel, E. Ünsal, M. Çakmak and Y.Z. Menceloğlu, "Improvement in gas permeability of biaxially stretched PET films blended with high barrier polymers: The role of chemistry and processing conditions," Eur. Polym. J., vol. 46, pp. 226-237, 2010.
- [26] A. Natu, E.A. Lofgren and S.A. Jabarin, "Effect of morphology on barrier properties of poly(ethylene terephthalate)," Polym. Eng. Sci., vol. 45, (3), pp. 400-409, 2005.

- [27] M. Hauptmann, "Die gezielte Prozessführung und Möglichkeiten zur Prozessüberwachung beim mehrdimensionalen Umformen von Karton durch Ziehen," Ph.D. Dissertation, Technische Universität Dresden, Dresden, Germany, 2010.
- [28] J.E. Sader, J.W.M. Chon and P. Mulvaney, "Calibration of rectangular atomic force microscope cantilevers," *Rev. Sci. Instrum.*, vol. 70, (10), pp. 3967–3969, 1999.
- [29] L.A. Baldenegro-Perez, D. Navarro-Rodriguez, F.J. Medellin-Rodriguez, B. Hsiao, C.A. Avila-Orta and I. Sics, "Molecular weight and crystallization temperature effects on poly(ethylene terephthalate) (PET) homopolymers, an isothermal crystallization analysis," *Polymers*, vol. 6, pp. 583–600, 2014.
- [30] O. Olabisi, "Conventional polyolefins," in *Handbook of thermoplastics*, O. Olabisi, Ed., CRC Press, Inc., 1997, pp. 1–38.
- [31] S. Fakirov, "Polyethylene terephthalate," In: Olabisi, O. (ed.), in *Handbook of thermoplastics*, O. Olabisi, Ed., CRC Press, Inc., 1997, pp. 449–464.
- [32] S.-S. Ovaska, P. Geydt, M. Österberg, L.-S. Johansson and K. Backfolk, "Heat-Induced changes in oil and grease resistant hydroxypropylated-starch-based barrier coatings," *Nord. Pulp Paper Res. J.*, vol. 30, (3), pp. 488–496, 2015.
- [33] B.A. Morris, "Understanding why adhesion in extrusion coating decreases with diminishing coating thickness, Part I: Penetration of porous substrates," *Proceedings of the TAPPI PLACE Conference*, 2006, Vol. 1, pp. 38–60.
- [34] E. Böhmer, "Thermal properties," in *Handbook of Physical Testing of Paper*, Vol. 2, J. Borch, M.B. Lyne, R.E. Mark and C. Habergel, Eds. New York: Marcel Dekker Inc., 2002, 560 p.
- [35] Goodfellow Corp., "Polyethylene terephthalate polyester (PET, PETP) - Properties and applications," [online] 2016, <http://www.azom.com/> (Accessed: 13 June 2016).
- [36] M. Hauptmann, M. Wallmeier, K. Erhard, R. Zelma and J.-P. Majschak, "The role of material composition, fiber properties and deformation mechanisms in the deep drawing of paperboard," *Cellulose*, vol. 22, pp. 3377–3395, 2015.
- [37] S. Allaoui, Z. Aboura and M.L. Benzeggagh, "Effects of the environmental conditions on the mechanical behaviour of the corrugated cardboard," *Compos. Sci. Technol.*, vol. 69, pp. 104–110, 2009.
- [38] A. Bolgov, "Effects of ambient conditions on dimensional stability and stiffness of commercial paperboard and paperboard trays," Master's Thesis, Lappeenranta University of Technology, Lappeenranta, Finland, 2015.